Human farnesyl pyrophosphate synthase inhibition by nitrogen bisphosphonates: A 3D-QSAR study

3 AUTHORS:

David Fernández Payeras
University of the Balearic Islands
7 PUBLICATIONS **40** CITATIONS

SEE PROFILE

Joaquin Ortega-Castro
University of the Balearic Islands
62 PUBLICATIONS **246** CITATIONS

SEE PROFILE

Juan Frau
University of the Balearic Islands
157 PUBLICATIONS **873** CITATIONS

SEE PROFILE

Human farnesyl pyrophosphate synthase inhibition by nitrogen bisphosphonates: a 3D-QSAR study

**David Fernández · Joaquín Ortega-Castro ·
Juan Frau**

Abstract We report the results of a comparative molecular field analysis and comparative molecular similarity index analysis of the human farnesyl pyrophosphate synthase (FPPS) inhibition by nitrogen bisphosphonates (NBPs) taking into account their time-dependent inhibition efficacies. The 3D-QSAR models obtained provide steric, electrostatic and hydrophobic contour maps consistent with the interactions into the active site of human FPPS observed in available crystallographic structures. Furthermore, the 3D-QSAR models obtained provide accurately IC_{50} values of the NBPs of the training set. The predictive ability of these 3D-QSAR models was found to rely on the choice of biologically active conformations of the target molecules and on a careful examination of the protonation status of the NBPs in the training set. The best models obtained can be useful to predict biological values of a high number of NBPs that have been used for the treatment of different diseases as potential inhibitors of the activity of the FPPS enzyme.

Keywords Bisphosphonates · 3D-QSAR · Human farnesyl pyrophosphate synthase · Inhibitors

D. Fernández · J. Ortega-Castro · J. Frau (✉)
Departament de Química, Institut Universitari d'Investigació en Ciències de la Salut (IUNICS), Universitat de les Illes Balears, Palma de Mallorca 07122, Spain
e-mail: juan.frau@uib.es

Introduction

Bisphosphonates (BPs) are a drug group (see Scheme 1), which emerged as inorganic pyrophosphate (PPi) analogues more than forty years ago, with a hydrolysis resistance of which facilitates their oral administration. BPs have been used to treat bone resorption related to conditions such as post-menopausal osteoporosis, Paget's disease and tumoral hypercalcemia [1–3]. These drugs have also been used against other diseases such as cancer [4–7] and found to possess antiparasitic, antibacterial and herbicidal action [8, 9].

The success of BPs in the treatment of bone resorption diseases relies on (*a*) their high affinity for bone surfaces in preference over other organs, (*b*) their being exclusively absorbed by osteoclasts (the cells affecting bone resorption) and (*c*) the rapid release of unabsorbed bisphosphonate molecules [10].

Nitrogen bisphosphonates (NBPs) are the most biologically active BPs group by virtue of their ability to inhibit the enzyme farnesyl pyrophosphate synthase (FPPS), which takes part in the mevanolate synthetic pathway. FPPS is a homodimeric enzyme that catalyses the condensation sequence of the allyl substrate, dimethylallyl pyrophosphate (DMAPP), with two molecules of 5-carbon isopentenyl pyrophosphate (IPP), to give C_{10} geranyl pyrophosphate (GPP) first and the isoprenoid C_{15} farnesyl pyrophosphate (FPP) later [11]. FPP is required to obtain geranylgeranyl pyrophosphate (GGPP) under the action of GGPP synthase. Both isoprenoids (FPP and GGPP) are indispensable metabolites for the post-translational modification (prenylation) of GTPases, which are responsible for anchoring proteins to cell membranes and play a prominent role in protein–protein interactions [12, 13]. Inhibition of FPPS reduces prenylation of GTPase proteins
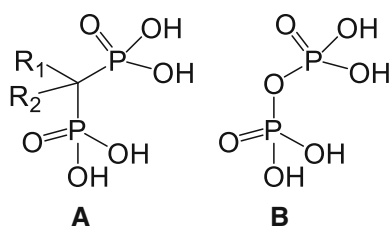
Scheme 1 **a** Basic structure of a bisphosphonic acid. **b** Structure of inorganic Pyrophosphate

and eventually brings cell metabolism to a halt [7, 14, 15]. Also, it leads to accumulation of the substrate isopentenyl diphosphate (IPP). IPP can be converted into ATP isopentenyl ester (ApppI), which induces cell apoptosis and increases the efficiency of BPs as a result [16]. The combination of both effects increases the biological activity of NBPs with respect to non-nitrogen BPs—the latter can only form non-hydrolysable derivatives of ATP (ApppI) [17].

Nitrogen bisphosphonates can bind to the active site of FPPS in competition with the allyl substrate DMAPP. Binding occurs by interaction of the phosphonate groups in NBPs with the cluster of three Mg^{2+} ions in between two aspartate-rich FPPS regions [16, 18–23]. The nitrogen atom in the R_2 side chain of the NBPs acquires the orientation required to form a hydrogen bond with the hydroxyl group in the Thr201 residue, and so does with the oxygen atom in the carbonyl group of Lys200. So NBPs occupy the hydrophobic hole that usually accommodates the isoprenoid lipid (GPP). Therefore, NBPs are direct competitors of DMAPP and GPP to form an enzyme–inhibitor complex at the active site. This results in a rapid inhibition of the enzymatic action and leads to slow isomerisation of the enzyme, which further inhibits it in a time-dependent manner.

3D-QSAR studies of the interactions between BPs and FPPS from various organisms such as *Trypanosoma brucei rhodesiense* [8], *Dyctiostelium discoideum* [24] and *Leishmania major* [25] have allowed the specific factors one can expect to govern the activity of NBPs as inhibitors of human FPPS to be roughly identified. These studies have shown that NBPs share some traits in their action on FPPS. However, Rondeau et al. [22] compared the crystallographic structure of human FPPS, which was elucidated in 2005, with those of the same enzyme from other species and identified substantial differences in their amino acid sequences. These studies revealed that FPPS from *Escherichia coli* and *Staphylococcus aureus* shared only 25 and 27 %, respectively, of the amino acid sequence of human FPPS. These differences additionally reflect major differences in conformation between human and non-human FPPS, and hence in the conditions and manner how the allyl substrate binds to the enzyme active site. A careful

study of the steric, electrostatic hydrophobic parameters governing the action of NBPs on human FPPS was therefore warranted.

Although BPs have been widely used, in the last years some studies showed that after a continued use, BPs may lead to weaker bones [26]. Some adverse effects are ocular inflammation, renal toxicity, ostenecrosis of jaw [27–29], and a higher risk of subtrochanteric or femoral shaft fractures [30].

With the purpose of obtaining a predictive 3D-QSAR model for the inhibition of human FPPS by NBPs, we considered two important aspects, the molecular conformations that NBPs can adopt within enzyme and its protonation state.

3D-QSAR models allow us to predict IC_{50} values of new NBPs and calculate IC_{50} values for human FPPS enzyme of NBPs that have been used in the treatment of other illnesses. Therefore, the 3D-QSAR model obtained allows us to identify anti-parasitic NBPs with least inhibitory effects on humans, useful in African trypanosomiasis (sleeping sickness) [8], and Chagas illness [24] and Leishmaniasis [25] treatments.

Furthermore, 3D-QSAR model gave us steric, electrostatics and hydrophobic requirements that regulate the biological activities of NBPs. These contour maps could be the starting point to design new family drugs in treatment of illnesses related with bone resorption. For example, polyphosphated molecules and polycarboxylic molecules, as citrate derivates, have a high affinity for the inorganic matrix of bone.

Methodology

A total of 20 NBPs of known initial and final IC_{50} values on human FPPS were used as training set [11]. The NBPs are depicted in scheme 2 and their biological activity on human FPPS, as IC_{50} values, is shown in Table 1. The NBPs spanned a wide range of R_2 side chains including alkylamino, cycloalkylamino and heteroaromatic groups. On the other hand, the R_1 side chain was either a hydrogen atom or a hydroxyl group.

The 3D-QSAR study, which was used to correlate the biological activity of the molecules in the training set with their structural, electrostatic and hydrogen-donor properties, was conducted by using the comparative molecular field analysis (CoMFA) method [31] and the comparative molecular similarity index analysis (CoMSIA) method [32]. These methods were previously used with success to examine the activity of BPs on *T. brucei* growth in trypomastigote blood [8], inhibition of *D. discoideum* growth [24], bone resorption [33] and *L. major* FPPS inhibition by BPs [25].

Scheme 2 Structures of NBPs investigated
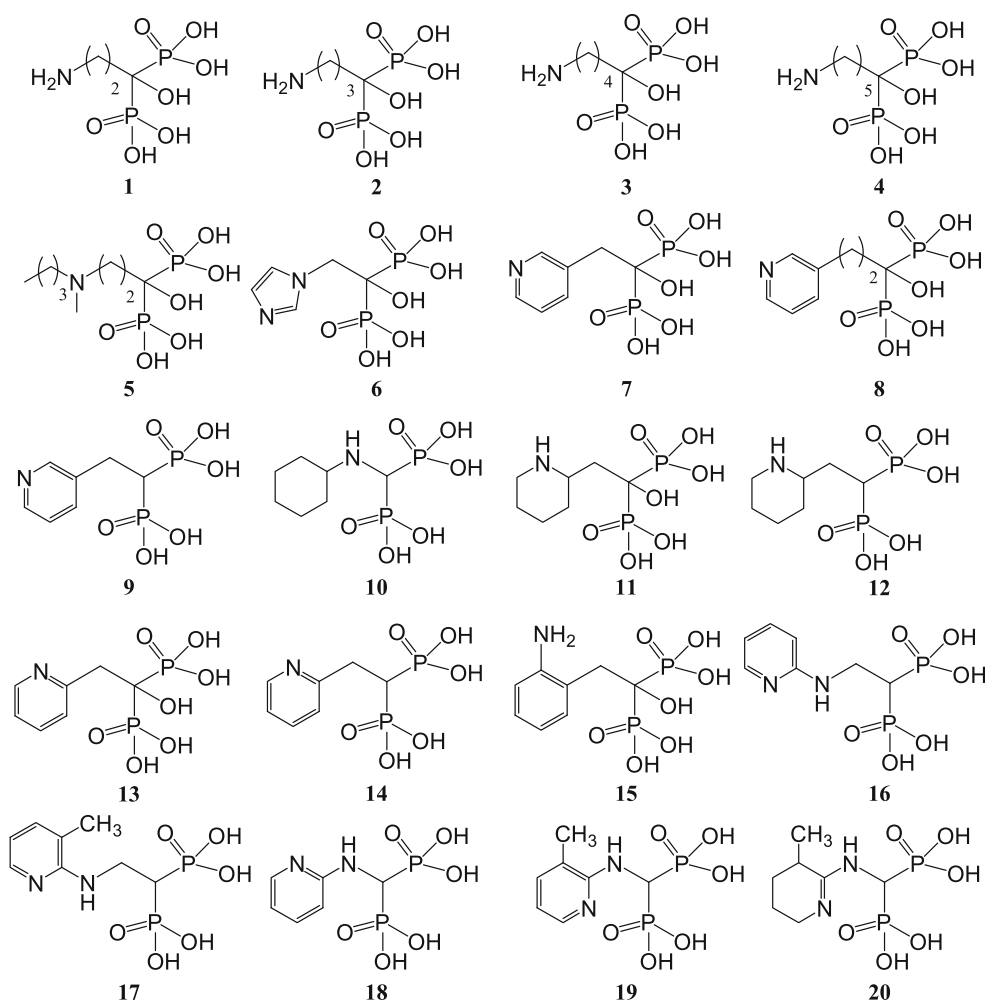
Nitrogen bisphosphonates structures were optimized by using a three-step protocol involving application of the steepest-descent, Powell and BFGS algorithms by using the Tripos force field [34] in the software Sybyl 8.0 [35]. Each energy-minimized structure was then aligned to the lowest conformation of risedronate (7) and each compound fitted to the (H)O–P–C–P–O(H) atoms in the bisphosphonate backbone common to all the NBPs. Natural orbital bond (NBO) [36–38] atomic charges for the minimized structures were calculated at Hartree–Fock level using 6–311 + G(d,p) basis set in Gaussian 09 program [39]. NBO atomic charges are appropriated to describe interactions between receptor and ligand molecules [40].

Comparative molecular field analysis descriptors were calculated as steric and electrostatic interactions between each molecule and a probe atom in a 3D rectangular grid with a 2 Å spacing around the molecule [41]. Similar to the CoMFA approach, a data table has been constructed from similarity indices calculated via a common probe atom which is placed at the intersections of a regularly spaced lattice. In the present CoMSIA study, three physicochemical properties have been evaluated: steric, electrostatic and hydrophobicity. The hydrophobicity factor has been calculated according to the parametrization of Viswanadhan [42].

Then, the 3D-QSAR/CoMFA and 3D-QSAR/CoMSIA equations were established by partial least-squares (PLS) analysis [43, 44] between biological activity and molecular parameters. The optimum number of components in the final equation was determined from the higher cross-validated q^2 value, which was calculated by using the leave-one-out (LOO) cross-validation technique.

The CoMFA and CoMSIA analyses were validated by performing a series of calculations to estimate the predictive value of the CoMFA and CoMSIA models. To this end, we excluded three compounds at random from the

Table 1 IC_{50} values for the inhibition of human FPPS by nitrogen bisphosphonates [11]

	Compound	Initial IC_{50} (nM)	Final IC_{50} (nM)
1	Pamidronate	1932	353.2
2	Alendronate	2,249	260.0
3	APHBP	1,079	298.5
4	Neridronate	2,427	388.2
5	Ibandronate	1,052	25.4
6	Zoledronate	475.3	4.1
7	Risedronate	452.9	5.7
8	NE58051	2,113	337.3
9	NE58043	173.4	32.6
10	YM-175	365.6	61.1
11	NE58027	591.6	13.7
12	NE58034	869.0	23.8
13	NE58018	349.1	9.2
14	NE97221	258.8	30.4
15	NE21650	370.7	21.6
16	NE11808	190.1	15.0
17	NE11809	988.6	734.5
18	NE11807	166.0	11.7
19	NE97220	75.2	6.2
20	NE58062	540.8	10.3

training set and constructed a new CoMFA/CoMSIA model that was used to predict the activity of the three compounds excluded. The process was performed three times to obtain a total of 9 predicted values and a mean absolute deviation (MAD).

The MAD of the prediction, together with r^2, q^2 and the standard error estimate (SEE), provided a measure of the quality of the CoMFA and CoMSIA models [45] and of whether it were accurate enough to reproduce and predict the activity of NBPs.

Results and discussion

Constructing an appropriate 3D-QSAR model required considering the biologically active conformations of the NBPs. Crystallographic data for enzyme–substrate complexes provide information about such conformations. However, the lack of such data for some NBPs required an additional conformational study.

The protein data bank (PDB) contains the crystallographic structures of human FPPS with various NBPs bound to its active site, namely: pamidronate (1) (PDB 2F89), alendronate (2) (PDB 2F92), ibandronate (5) (PDB 2F94) [22], zoledronate (6) (PDB 2F8C) and risedronate (7) (PDB 1YV5, 1YQ7) [21]. This crystallographic information was used to identify the biologically active

conformations of the other NBPs studied. The structure of risedronate (7 in scheme 2) was used as reference for the conformations of the NBPs (6)–(20), which had an aromatic or non-aromatic cycle in R_2 (Fig. 1). Three different models where considered for the conformations of (1)–(5) structures.

Model A We initially used a training set where all NBPs with an aliphatic side chain (1)–(5) were in their extended conformation. This methodology was previously used by Sanders et al. [25] to examine the activity of BPs on *Leishmania* FPPS. Figure 2a shows the molecular arrangement of the structures possessing aliphatic side chains in accordance with the model.

Model B This model was constructed from the crystallographic structures of pamidronate (1), alendronate (2) and ibandronate (5) plus a contracted conformation of the aliphatic side chains R_2 in (3) and (4). The contracted conformation had its terminal nitrogen atoms in a spatial region similar to that in the crystallographic structures of (1) and (2). Figure 2b shows the molecular arrangement of structures (1)–(5) in accordance with this model.

Model C This model was a combination of the previous two and constructed from the crystallographic conformations of (1), (2) and (5) plus the extended conformations of (3) and (4). Figure 2c shows the molecular arrangement of structures (1) to (5) in accordance with this model.

Other variable to be considered in addition to the configuration of the R_2 chain in the NBPs was the protonation status of the nitrogen atom in the chain. At physiological pH, a molecular chain may be protonated and influence the parameters of the CoMFA and CoMSIA models and pIC_{50} predictions. This led us to construct four new models from each of the previous three. These new models additionally considered the protonation status of the NBPs structures of the training set at physiological pH.
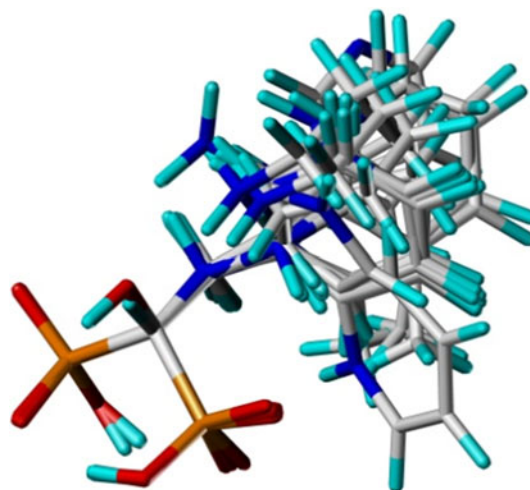
Fig. 1 Alignment of nitrogen bisphosphonates with cyclic side chains (molecules 6–20)
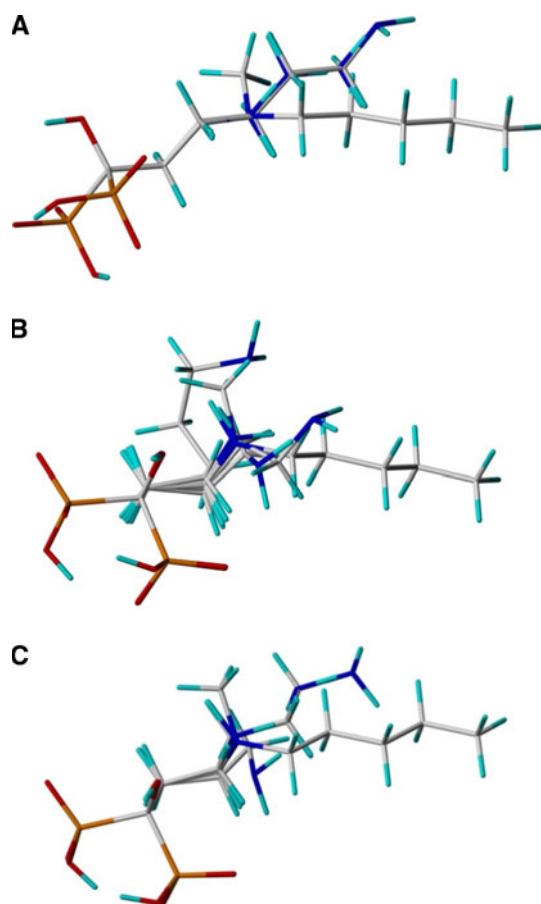
Fig. 2 a Alignment of nitrogen bisphosphonates with the extended aliphatic side chain (molecules 1–5) from model A. **b** Alignment of molecules (1)–(5) from model B. **c** Alignment of molecules (1)–(5) from model C

Table 2 Protonation of R_2 groups according to the considered models

	pKa	Physiologic pH	X	X1	X2	X3	X4
Amine	~10[a]	100 % protonated	No	Yes	Yes	Yes	Yes
Imidazole	7.05[b]	~50 % protonated	No	No	Yes	No	Yes
2-aminopyr-idine	6.82[a]	~50 % protonated	No	No	No	Yes	Yes
Pyridine	5.25[a]	~0 % protonated	No	No	No	No	No
Aniline	4.63[a]	~0 % protonated	No	No	No	No	No

[a] Ref. [48]. [b] Ref [49]

Table 3 3D-QSAR/CoMFA statistical results for different models obtained with NBO atomic charges and initial IC_{50} values

Model	N[a]	$q^{2,\,b}$	$r^{2,\,c}$	F[d]	SEE[e]	MAD[f]	Steric[g]	Elect.[h]
A	4	0.689	0.969	116	0.08	0.23	91.2	8.8
A1	5	0.759	0.983	165	0.06	0.27	81.3	18.7
A2	5	0.754	0.984	174	0.06	0.30	81.8	18.2
A3	3	0.721	0.931	72	0.12	0.20	72.2	27.8
A4	3	0.720	0.929	69	0.12	0.20	73.3	26.7
B	2	0.642	0.842	45	0.18	0.25	94.0	6.0
B1	7	0.783	0.992	215	0.05	0.21	78.9	21.1
B2	7	0.789	0.992	216	0.05	0.19	80.9	19.1
B3	3	0.719	0.949	100	0.10	0.16	74.4	25.6
B4	4	0.733	0.961	92	0.09	0.17	75.0	25.0
C	4	0.643	0.969	117	0.08	0.21	91.1	8.9
C1	5	0.799	0.986	195	0.06	0.17	79.1	20.9
C2	5	0.794	0.986	201	0.06	0.15	80.4	19.6
C3	4	0.709	0.956	82	0.10	0.16	73.0	27.0
C4	4	0.725	0.957	83	0.10	0.15	74.8	25.2

[a] N = number of components in CoMFA model. [b] q^2: Cross-validated correlation coefficient after leave-one-out procedure. [c] r^2: Correlation coefficient. [d] F_{test} = Fischer test. [e] SEE: standard error of estimated values. [f] MAD: Mean Absolute Deviation of 9 predicted values in test sets. [g] Steric: contribution of steric parameters in 3D-QSAR model. [h] Elect.: contribution of electrostatic parameters in 3D-QSAR model

The first protonated models (Table 2), which were designated X1 (where X represents A, B or C) assumed the nitrogen atom of the amino group ($pK_a \approx 10$) in the R_2 side chains of NBPs (1)–(5) and (10)–(12) and the nitrogen of R_2 in (20), the pK_a for which was previously calculated to be 9.56 [46] and 10.61 [47], to be protonated. X2 models also included the protonation of the nitrogen atom of the imidazole group ($pK_a = 7.05$) in the side chain of zoledronate (6). X3 models assumed 2-aminopyridine derivatives [i.e. molecules (16)–(19)] to be protonated and the imidazole derivative (6) unprotonated. Finally, X4 models included the assumptions of X1, X2 and X3. Structures (7), (8), (9), (13) and (14) (i.e. pyridine derivatives, with $pK_a = 5.3$), and molecule (15), which possessed an aniline group in R_2 ($pK_a = 4.6$), were assumed to be unprotonated in all models.

3D-QSAR models with initial IC_{50} values

Table 3 shows the statistical results, and the steric and electrostatic parameters, of the fifteen CoMFA models

obtained, taking into account initial IC_{50} values. The results of the different CoMFA analyses are included in the Supplementary Material.

To choose the best model for the study we considered the following items: (1) number of components in the QSAR equation, (more than 6 components is related with over-fitting phenomena); (2) good values for q^2 and r^2 parameters [50]; (3) good results in the prediction tests (SEE and MAD); (4) the contour maps which more accurately describe the interactions into the active site.

Table 4 3D-QSAR/CoMFA results of C4 model obtained with NBO atomic charges and initial IC_{50} values

Compounds	Experimental		Predicted human FPPS pIC_{50} values			
	Initial IC_{50} (nM)	pIC_{50}	Training	Test sets		
				1	2	3
1	1,932 ± 152.6	5.71	5.77	5.75	5.76	5.76
2	2,249 ± 180	5.65	5.62	5.64	5.61	5.62
3	1,079 ± 82.1	5.97	5.82	**5.69**	5.85	5.90
4	2,427 ± 147	5.61	5.72	5.61	5.75	5.70
5	1,052 ± 55.1	5.98	6.00	5.94	**6.14**	5.96
6	475.3 ± 18.3	6.32	6.25	6.31	6.25	6.33
7	452.9 ± 16.6	6.34	6.45	6.43	6.45	6.48
8	2,113 ± 188	5.68	5.58	5.67	5.59	**5.69**
9	173.4 ± 10.5	6.76	6.61	6.64	6.64	6.55
10	365.6 ± 32	6.44	6.50	6.52	6.47	**6.45**
11	591.6 ± 91.6	6.23	6.15	6.21	**6.04**	6.20
12	869.0 ± 77.0	6.06	6.21	**6.30**	6.14	6.08
13	349.1 ± 22.7	6.46	6.48	6.45	6.46	**6.57**
14	258.8 ± 21.2	6.59	6.62	6.62	**6.61**	6.61
15	370.7 ± 14.3	6.43	6.52	6.46	6.52	6.47
16	190.1 ± 22.5	6.72	6.68	6.74	6.71	6.78
17	988.6 ± 50.6	6.00	6.03	6.01	6.01	5.99
18	166.0 ± 15.3	6.78	6.83	6.74	6.85	6.82
19	75.2 ± 4.6	7.12	7.00	**6.77**	7.01	7.10
20	540.8 ± 16.9	6.27	6.28	6.24	6.26	6.24
	$q^{2,a}$		0.725	0.734	0.733	0.630
	$r^{2,b}$		0.957	0.985	0.965	0.97
	N^c		4	5	4	5
	F^d_{test}		83	149	82	70
	n^e		20	17	17	17
	SEE^f		0.10	0.06	0.10	0.09
	Field contributions					
	Steric		74.8	71.7	74.6	75.4
	Electrostatic		25.2	28.3	25.4	24.6
	MAD^g				0.15	

Bold values in the test sets stands by the predicted activity of this compound, which has been excluded to construct a new CoMFA model

[a] q^2: Cross-validated correlation coefficient after leave-one-out procedure. [b] r^2: Correlation coefficient. [c] N = number of components in CoMFA model. [d] F: Fisher test. [e] n: number of molecules in the training or test sets. [f] SEE: standard error of estimated values. [g] MAD: Mean Absolute Deviation of 9 predicted values in test sets

The three models show similar statistical parameters. Protonation in the nitrogen atom in the side chain R_2 of the molecules in the training set (X1, X2, X3, X4 models) improves the statistical results and increases the significance of electrostatic factors. In any case, the biological activity of the molecules was more markedly dependent on steric factors than on electrostatic factors. When we consider the contour maps, the C4 model is slightly better. For this reason, the discussion of the results is based on C4 model. However in terms of statistical results C1 and C2 models could also be considered.

Table 4 shows the 3D-QSAR/CoMFA results obtained with C4 model. In this model the amino group, imidazole and 2-aminopyridine derivates were protonated. This model exhibited a q^2 value of 0.725, and an r^2 value of 0.957; used 4 regression components; a good Fischer's test value (F = 83); and a predicted pIC_{50} (SEE) of 0.10. Model C4 was used to predict nine different molecules via different test sets; the MAD in the predictions was 0.15 pIC_{50} units. Table 4 shows the contribution of steric and electrostatic interactions to the model (74.8 and 25.2 %, respectively).

Table 5 3D-QSAR/CoMSIA results of C4 model obtained with NBO atomic charges and initial IC_{50} values

Compounds	Experimental		Predicted human FPPS pIC_{50} values			
	Initial IC_{50} (nM)	pIC_{50}	Training	Test sets		
				1	2	3
1	1,932 ± 152.6	5.71	5.86	5.87	5.74	5.89
2	2,249 ± 180	5.65	5.64	5.70	5.66	5.75
3	1,079 ± 82.1	5.97	5.96	**5.71**	5.95	5.73
4	2,427 ± 147	5.61	5.65	5.51	5.62	5.61
5	1,052 ± 55.1	5.98	6.02	6.14	**6.03**	6.07
6	475.3 ± 18.3	6.32	6.32	6.18	6.31	6.18
7	452.9 ± 16.6	6.34	6.43	6.32	6.36	6.37
8	2,113 ± 188	5.68	5.60	5.74	5.70	**6.08**
9	173.4 ± 10.5	6.76	6.63	6.68	6.72	6.68
10	365.6 ± 32	6.44	6.41	6.55	6.44	**6.43**
11	591.6 ± 91.6	6.23	5.96	6.01	**5.67**	5.98
12	869.0 ± 77.0	6.06	6.19	**6.40**	6.03	6.32
13	349.1 ± 22.7	6.46	6.51	6.40	6.44	**6.43**
14	258.8 ± 21.2	6.59	6.71	6.75	**6.81**	6.73
15	370.7 ± 14.3	6.43	6.50	6.40	6.42	6.44
16	190.1 ± 22.5	6.72	6.68	6.69	6.72	6.67
17	988.6 ± 50.6	6.00	5.99	6.17	6.00	6.34
18	166.0 ± 15.3	6.78	6.88	6.70	6.89	6.80
19	75.2 ± 4.6	7.12	6.95	**6.66**	7.08	6.86
20	540.8 ± 16.9	6.27	6.20	6.16	6.26	6.13
	$q^{2, a}$		0.586	0.599	0.767	0.516
	$r^{2, b}$		0.943	0.913	0.994	0.838
	N^c		4	2	6	2
	F_{test}^d		63	73	279	36
	n^e		20	17	17	17
	SEE^f		0.11	0.13	0.04	0.19
	Field contributions					
	Steric		27.8	24.2	25.2	20.7
	Electrostatic		16.4	17.7	17.3	17.7
	Hydrophobicity		55.7	58.0	57.5	61.6
	MAD^g		**0.26**			

Bold values in the test sets stands by the predicted activity for this compound, which has been excluded to construct a new CoMSIA model

[a] q^2: Cross-validated correlation coefficient after leave-one-out procedure. [b] r^2: Correlation coefficient. [c] N = number of components in CoMSIA model. [d] F: Fisher test. [e] n: number of molecules in the training or test sets. [f] SEE: standard error of estimated values. [g] MAD: Mean Absolute Deviation of 9 predicted values in test sets

The 3D-QSAR/CoMSIA results obtained for the model C4 are shown in Table 5. The highest cross-validated value $q^2 = 0.586$ was obtained for four components with a non cross-validated r^2 value of 0.943, Fischer's test value F = 63, and standard error of pIC_{50} estimated values (SEE) of 0.11 (Table 5). The MAD in the predictions was 0.26 pIC_{50} units, higher than MAD value obtained for CoMFA model. It can be observed that statistical results are slightly inferior that the ones obtained in the CoMFA study. The steric, electrostatic and hydrophobic fields contributions were 27.8, 16.4 and 55.7 %, respectively. According to the CoMSIA model, the biological activity of the molecules was markedly dependent on hydrophobicity factors than on steric or electrostatic factors.

In these models electrostatic contribution on QSAR equations are high enough to justify a carefully study of the atomic charge types effects on statistical results. In this work, we performed a CoMFA/CoMSIA studies with Gasteiger-Marsili [51, 52], Mulliken [53, 54], Merz-Kollman [55, 56], CHelpG [57] and NBO [36–38] atomic charges. In Merz-Kollman and ChelpG methods the atomic charges are fitted to electrostatic surface potential whereas NBO

Table 6 3D-QSAR statistical results obtained for different atomic charge types and initial IC_{50} values

Parameters	Gasteiger-Marsili		Mulliken		Merz-Kollman		CHelpG		NBO	
	CoMFA	CoMSIA	CoMFA	CoMSIA	CoMFA	CoMSIA	CoMFA	CoMSIA	CoMFA	CoMSIA
N^a	5	4	5	2	4	3	4	3	4	4
$q^{2, b}$	0.720	0.586	0.714	0.549	0.725	0.568	0.724	0.564	0.725	0.586
$r^{2, c}$	0.970	0.932	0.978	0.865	0.957	0.918	0.957	0.916	0.957	0.943
F^d	91	51	126	55	83	60	83	58	83	63
SEE^e	0.08	0.12	0.07	0.16	0.10	0.13	0.10	0.13	0.10	0.11
MAD^f	0.17	0.27	0.17	0.29	0.15	0.27	0.16	0.28	0.15	0.26
Steric	76.4	26.8	71.6	19.0	75.5	22.8	76.3	24.6	74.8	27.8
Electrostatic	23.6	14.6	28.4	27.0	24.5	22.9	23.7	17.5	25.2	16.4
Hydrophobicity	–	58.6	–	54.0	–	54.3	–	57.9	–	55.7

[a] N = number of components in CoMFA/CoMSIA model. [b] q^2: Cross-validated correlation coefficient after leave-one-out procedure. [c] r^2: Correlation coefficient. [d] F: Fisher test. [e] SEE: standard error of estimated values. [f] MAD: Mean Absolute Deviation of 9 predicted values in test sets

method describes the N-electron wavefunction in terms of localized orbitals or configurations which are closely tied to chemical bonding concepts. Table 6 shows statistical results and as can be seen the best results correspond to Merz-Kollman, ChelpG and NBO atomic charges, although there are not significant differences between them in CoMFA and CoMSIA studies.

Molecular field

The CoMFA parameters calculated with model C4 were used to construct three-dimensional graphs of the steric and electrostatic fields (Fig. 3). The spatial regions where steric interactions in the NBPs were favourable are shown in green and those where interactions were unfavourable -and biological activity reduced as a result- in yellow. Figure 3 shows the favourable and unfavourable steric regions projected into the active site of the human FPPS enzyme complexed with zoledronate (6) (PDB 2F8Z). Zoledronate binds to the active site by electrostatic interactions between the phosphonate groups with the three cations (in this case Mg^{2+}). These cations show an octahedral coordination with the phosphonate groups of inhibitor, the carboxylate groups of Asp103, Asp107 and Asp243 residues, and some water molecules (water molecules are not represented in Fig. 3). NBPs are also stabilized into the active site by direct salt bridge interactions between phosphonate groups of the inhibitor and residues Arg112, Lys200 and Lys257. These interactions have also been found in the crystallographic structures of: pamidronate (PDB: 2F89), alendronate (PDB 2F92), ibandronate (PDB 2F94) and risedronate (PDB 1YV5). Figure 3b shows the R_2 side chain of zoledronate oriented to a favourable steric region (green). This region is included into the hydrophobic cavity [58] defined by the residues: Phe99, Leu100, Thr167, Gln171,

Tyr199, Lys200, Thr201, Tyr204, Phe239, and oriented to the area between Thr167, Gln171 and the side chain of Lys200.The IPP cofactor completes the hydrophobic site, enclosing the inhibitor into the cavity [11]. The crystallographic structure of zoledronate into the active site with IPP (PDB: 2F8Z) and without IPP (PDB: 2F8C) did not show significant differences of the hydrophobic cavity of the active site.

For the case of zoledronate, the nitrogen in R_2 forms a hydrogen bond to Lys200 and Thr201 amino acids, whereas the hydroxyl group (R_1) bonds to Asp243 at the active site of human FPPS. This can be easily inferred by comparing the electrostatic contour map with the X-ray structure for zoledronate at the enzyme active site (see Fig. 3b). The blue regions in the contour map are those where the presence, in the molecule, of negative charge or a hydrogen bond acceptor group is favourable and of positive charge or a hydrogen bond donor is unfavourable. Conversely, the red regions are those where the presence of positive charge or a hydrogen bond donor group is favourable.

The contour maps are consistent with the data in Table 1. The molecule with the greatest inhibitory action among the NBPs was (19) and that with the smallest neridronate (4). Neridronate has a hydroxyl group oriented to an unfavourable steric region, and a protonated amino group not oriented to a favourable electrostatic region. It exhibited the poorest initial IC_{50} value (2,427 nM) (see Fig. 4). However, the projection of neridronate into the active site of FPPS enzyme could suggest some weak hydrogen bond with the carbonyl group of Lys200. In molecule (19), the protonated aromatic nitrogen is not perfectly oriented to an electrostatically favourable region; however, its steric interaction is highly favourable (see Fig. 4), and the net result is the highest initial biological activity among all NBPs studied (initial IC_{50} = 75.2 nM).
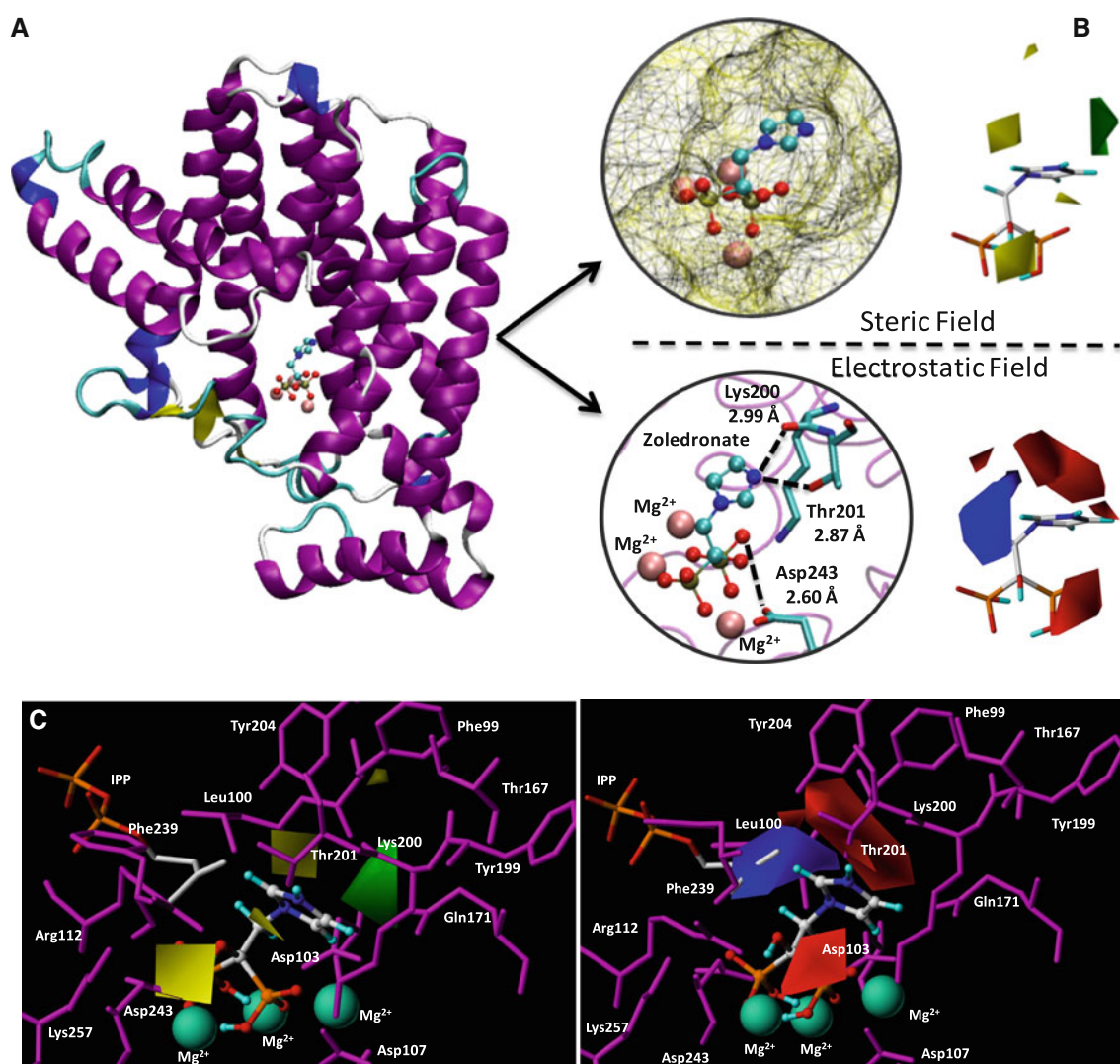
Fig. 3 a Binding of zoledronate (6) to human FPPS (PDB 2F8Z). **b** 3D-QSAR/CoMFA model C4 steric and electrostatic fields. Green regions indicate where steric bulk is expected to enhance activity; *yellow regions* indicate where steric bulk is expected to reduce activity. *Red regions* indicate where positive charge in the molecule is expected to enhance activity; *blue region* indicate where negative charge in the molecule is expected to enhance activity. **c** Zoledronate (6), favourable and unfavourable contour maps projected into the active site of the human FPPS enzyme (PDB 2F8Z)

As can be seen from Table 1, the NBPs with an aliphatic R_2 side chain [i.e. molecules (1)–(5)] were the least active, and hence exhibited the highest IC_{50} initial values (1,052–2,427 nM). In the steric contour map (Fig. 5), R_2 in these molecules was oriented to sterically unfavourable (yellow) regions established by the CoMFA model. In the electrostatic contour map obtained with CoMFA model, the protonated amino groups of pamidronate (1) and alendronate (2) are not oriented towards a favourable electrostatic red region, although PDB structures (PDB 2F89 and 2F92, respectively) could suggest some weak hydrogen bond with Tyr204, instead of Lys200 and Thr201 residues. Combination of these steric and electrostatic contour maps can explain the low biological activity of these compounds.

The APHBP molecule (3), which possesses one more atom in the R_2 chain, exhibited a higher biological activity than pamidronate (1) and alendronate (2). Unlike the latter two, APHBP had an extended conformation in its R_2 side chain which departed from the sterically unfavourable region (see Fig. 5). Furthermore, the terminal amino group could be located in an electrostatic favourable region close to Lys200 and Tyr204. A subsequent increase of the number of atoms in the side chain moves the protonated amino group away from electrostatic favourable region, and decreases the biological activity of the NBPs (e.g. in neridronate, with $IC_{50} = 2,427$ nM).

However, increasing the length of the molecule not necessarily reduced biological activity; thus, ibandronate
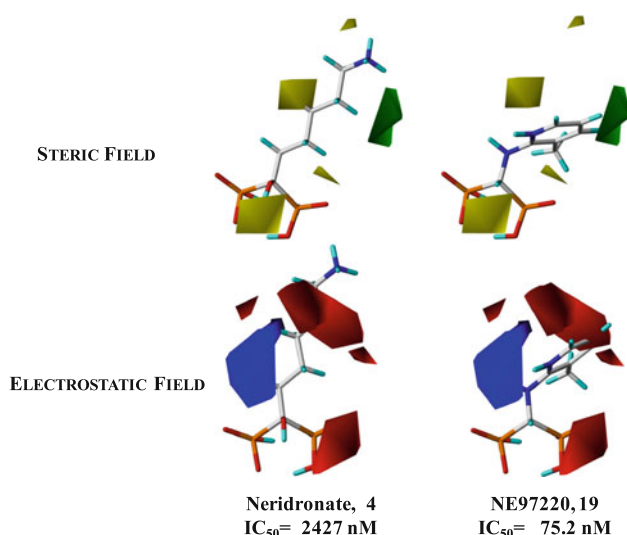
Fig. 4 IC_{50} values analysis of neridronate (4) and molecule (19) (NE97220) and steric and electrostatic fields from model C4. *Green regions* indicate where steric bulk is expected to enhance activity; *yellow regions* indicate where steric bulk is expected to reduce activity. *Red regions* indicate where positive charge is expected to enhance activity; *blue region* indicate where negative charge is expected to enhance activity

Fig. 6 IC_{50} values analysis of risedronate (7) and molecule (8) and steric and electrostatic field from model C4. *Green regions* indicate where steric bulk is expected to enhance activity; *yellow regions* indicate where steric bulk is expected to reduce activity. *Red regions* indicate where positive charge is expected to enhance activity; *blue region* indicate where negative charge is expected to enhance activity

(5) (1,052 nM) has a side chain longer than neridronate (4) (2,427 nM), as a result of R_2 occupying sterically favourable region. A closer look at the active site of the FPPS complexed with ibandronate (PDB 2F94) shows the R_2 side chain oriented to the region between Gln171 and Phe99 residues. This region shows a Gln171 and Phe99 distance higher (2 Å more than in zoledronate and risedronate
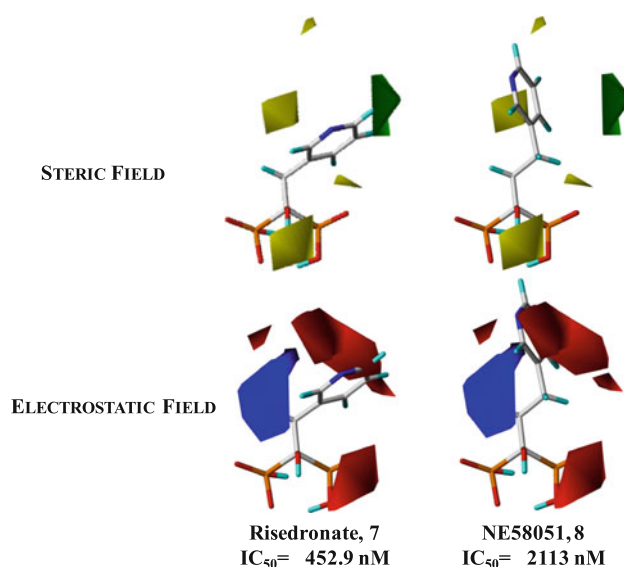
complexed to FPPS) and allows to relocate the R_2 side chain. This fact is also observed in other NBPs with large R_2 side chain, for example YS0470 (PDB: 4H5C) not included in the training set.

The NBPs possessing one atom between an aromatic ring and the P–C–P backbone were those most tightly fitted
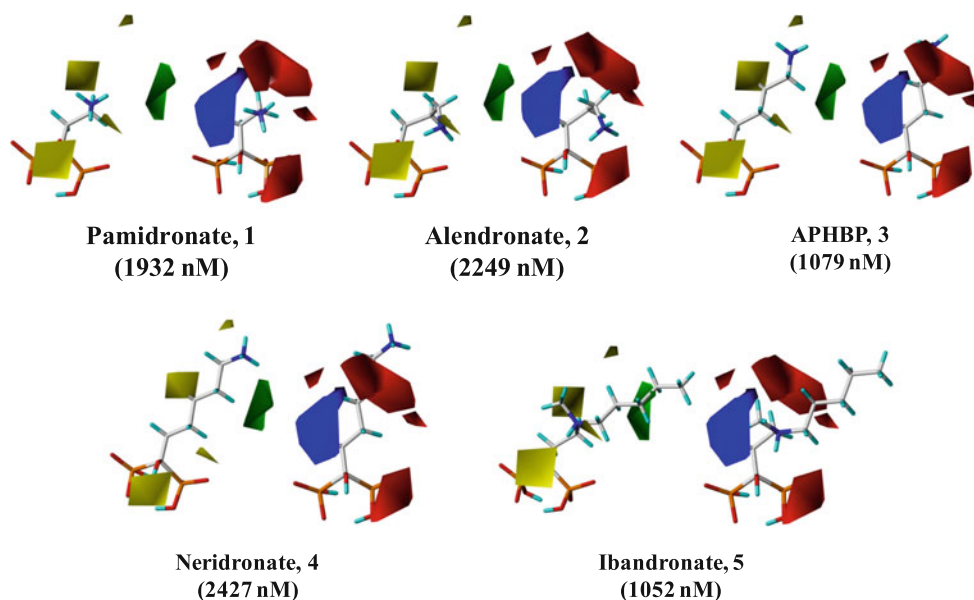

Fig. 5 Steric and electrostatic map fields for pamidronate (1), alendronate (2), APHBP (3), neridronate (4) and ibandronate (5). *Green regions* indicate where steric bulk is expected to enhance activity; *yellow regions* indicate where steric bulk is expected to reduce activity. *Red regions* indicate where positive charge is expected to enhance activity; *blue region* indicate where negative charge is expected to enhance activity
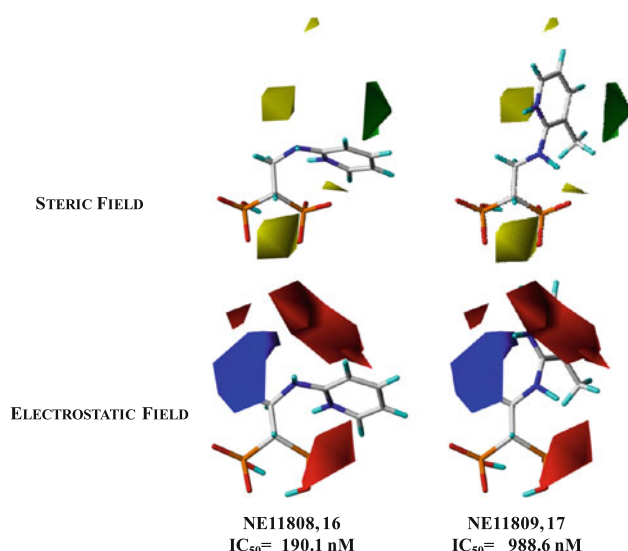
Fig. 7 IC_{50} values analysis of NE11808 (16) and NE11809 (17) and steric and electrostatic field from model C4. *Green regions* indicate where steric bulk is expected to enhance activity; *yellow regions* indicate where steric bulk is expected to reduce activity. *Red regions* indicate where positive charge is expected to enhance activity; *blue region* indicate where negative charge is expected to enhance activity

into the active site. As a consequence, these NBPs (6), (7), (9), (13)–(15), (18) and (19) exhibited low initial IC_{50} values. In many cases, this was the result of the ring rigidity causing the aromatic nitrogen and the oxygen atom in the carbonyl group to adopt a suitable conformation for hydrogen bonding to Thr201 and/or Lys200, which facilitated electrostatic interactions and the binding of NBPs to the active site of FPPS.

The presence of an aromatic ring not always has a low IC_{50} value. Thus, the only difference between risedronate (7) and molecule (8) is the distance between the ring and the P–C–P backbone. Molecule (8) shows a very low

biological activity (IC_{50} = 2,113 nM) due to the ring ceasing to occupy a sterically favourable spatial region (Fig. 6).

Finally, molecule (16) (Fig. 7) has an initial IC_{50} value of 190.1 nM, much lower than molecule (17) (initial IC_{50} value of 988.6 nM). This difference is caused by the distinct orientation of the aromatic ring of respective side chains. The presence of one methyl group orientates the aromatic ring to an unfavourable steric region, inducing a decrease of biological activity of molecule (17).

Time-dependent inhibition efficacy of NBPs

Preincubation of the NBPs with FPPS resulted in a decrease in IC_{50} values [11]. After 10 min of preincubation it was observed that IC_{50} values decrease between 25 % for molecule (17), and 99 % for zoledronate (6) and risedronate (7). The increase in inhibition has been explained by Dunford et al. [11] due to the isomerization of the enzyme-inhibitor complex.

Comparative molecular field analysis analyses have been done for the fifteen models using the final IC_{50} values. In all cases, we also observed an improvement with the introduction of protonation of R_2 side chain (X1, X2, X3 and X4 models) (Supplementary Material). Table 7 shows the CoMFA and CoMSIA statistical results, and the steric, electrostatic and hydrophobicity parameters, of the best models obtained with final IC_{50} values. The best pair of CoMFA/CoMSIA results was obtained for model A4. This model shows the extended conformation of side chain for molecules (1) and (2), and also the protonation of amino, imidazole and 2-aminopyridine groups.

The 3D-QSAR/CoMSIA results obtained for the model A4 are shown in Table 8. The highest cross-validated value $q^2 = 0.673$ was obtained for six components with a non

Table 7 Statistical results obtained for CoMFA/CoMSIA analysis for A1, A2, A4 and C1 models with final IC_{50} values

Parameters	A1		A2		A4		C1	
	CoMFA	CoMSIA	CoMFA	CoMSIA	CoMFA	CoMSIA	CoMFA	CoMSIA
N^a	6	7	5	7	7	6	5	2
$q^{2, b}$	0.681	0.553	0.700	0.592	0.680	0.673	0.614	0.404
$r^{2, c}$	0.987	0.993	0.976	0.991	0.992	0.988	0.981	0.772
F^d	164	230	112	192	208	178	141	29
SEE^e	0.10	0.08	0.13	0.08	0.08	0.10	0.12	0.36
MAD^f	0.37	0.36	0.35	0.39	0.44	0.23	0.35	0.37
Steric	73.4	23.2	72.0	25.2	67.7	27.8	68.7	30.3
Electrostatic	26.6	21.0	28.0	19.4	32.3	23.2	31.3	22.1
Hydrophobicity	–	55.8	–	55.4	–	49.0	–	47.6

[a] N = number of components in CoMFA/CoMSIA model. [b] q^2: Cross-validated correlation coefficient after leave-one-out procedure. [c] r^2: Correlation coefficient. [d] F: Fisher test. [e] SEE: standard error of estimated values. [f] MAD: Mean Absolute Deviation of 9 predicted values in test sets

cross-validated r^2 value of 0.988, Fischer's test value F = 178, and standard error of pIC_{50} estimated values (SEE) of 0.10. The MAD in the predictions was 0.23 pIC_{50} units. The steric, electrostatic and hydrophobic field contributions were 27.8, 23.2 and 49.0 %, respectively.

Figure 8 shows the molecular map field obtained with the CoMSIA parameters of model A4, projected into the active site of the human FPPS enzyme (PDB 2F8Z). Figure 8a shows the R_2 side chain of molecule (19) oriented to a favourable steric region (green). This region is contained in the zone between Thr167, Gln171 and the side chain of

Lys200. Unfavourable steric region (yellow) is located into the limit of cavity formed by the side chains of Tyr204, Phe99 and Thr167. This location corresponds to the orientation of the side chains of molecules (1)–(4), (8) and (17), and it is in agreement with their low values of biological activity.

Figure 8b shows the projection of favourable and unfavourable electrostatic region into the active site of the enzyme. This contour map is different from electrostatic contour map obtained with CoMFA analysis and initial IC_{50} values. Electrostatic favourable region for a positive

Table 8 3D-QSAR/CoMSIA results of A4 model obtained with NBO atomic charges and final IC_{50} values

Compounds	Experimental		Predicted human FPPS pIC_{50} values			
	Final IC_{50} (nM)	pIC_{50}	Training	Test sets		
				1	2	3
1	353.2 ± 32.1	6.45	6.46	6.45	6.47	6.44
2	260.0 ± 19.6	6.58	6.59	6.56	6.58	6.61
3	298.5 ± 36.6	6.52	6.44	**6.22**	6.43	6.48
4	388.2 ± 23	6.41	6.46	6.42	6.48	6.45
5	25.4 ± 1.57	7.60	7.61	7.62	**8.33**	7.63
6	4.1 ± 0.22	8.39	8.50	8.49	8.53	8.46
7	5.7 ± 0.54	8.24	8.05	8.09	8.02	8.04
8	337.3 ± 77	6.47	6.51	6.49	6.53	**6.74**
9	32.6 ± 2	7.49	7.61	7.66	7.62	7.65
10	61.1 ± 5.1	7.21	7.17	7.14	7.13	**7.19**
11	13.7 ± 0.9	7.86	7.90	7.88	**7.91**	7.87
12	23.8 ± 2.5	7.62	7.50	**7.46**	7.54	7.53
13	9.2 ± 0.96	8.04	7.94	7.95	7.97	**7.83**
14	30.4 ± 2.0	7.52	7.49	7.50	**7.56**	7.44
15	21.6 ± 2,8	7.67	7.76	7.68	7.78	7.74
16	15.0 ± 3.3	7.82	7.84	7.84	7.80	7.81
17	734.5 ± 48.9	6.13	6.16	6.16	6.17	6.15
18	11.7 ± 3.1	7.93	7.98	7.92	7.97	7.97
19	6.2 ± 1.45	8.21	8.17	**7.94**	8.16	8.19
20	10.3 ± 0.5	7.99	8.01	7.97	8.04	8.01
	$q^{2,\ a}$		0.673	0.637	0.690	0.439
	$r^{2,\ b}$		0.988	0.990	0.985	0.988
	N^c		6	6	5	6
	F_{test}^d		178	167	143	137
	n^e		20	17	17	17
	SEE^f		0.10	0.09	0.11	0.10
	Field contributions:					
	Steric		27.8	28.1	28.6	24.9
	Electrostatic		23.2	23.0	21.1	23.8
	Hydrophobicity		49.0	48.9	50.3	51.3
	MAD^g			**0.23**		

Bold values in the test sets stands by the predicted activity for this compound, which has been excluded in the new CoMSIA model

[a] q^2: Cross-validated correlation coefficient after leave-one-out procedure. [b] r^2: Correlation coefficient. [c] N = number of components in CoMSIA model. [d] F: Fisher test. [e] n: number of molecules in the training or test sets. [f] SEE: standard error of estimated values. [g] MAD: Mean Absolute Deviation of 9 predicted values in test sets
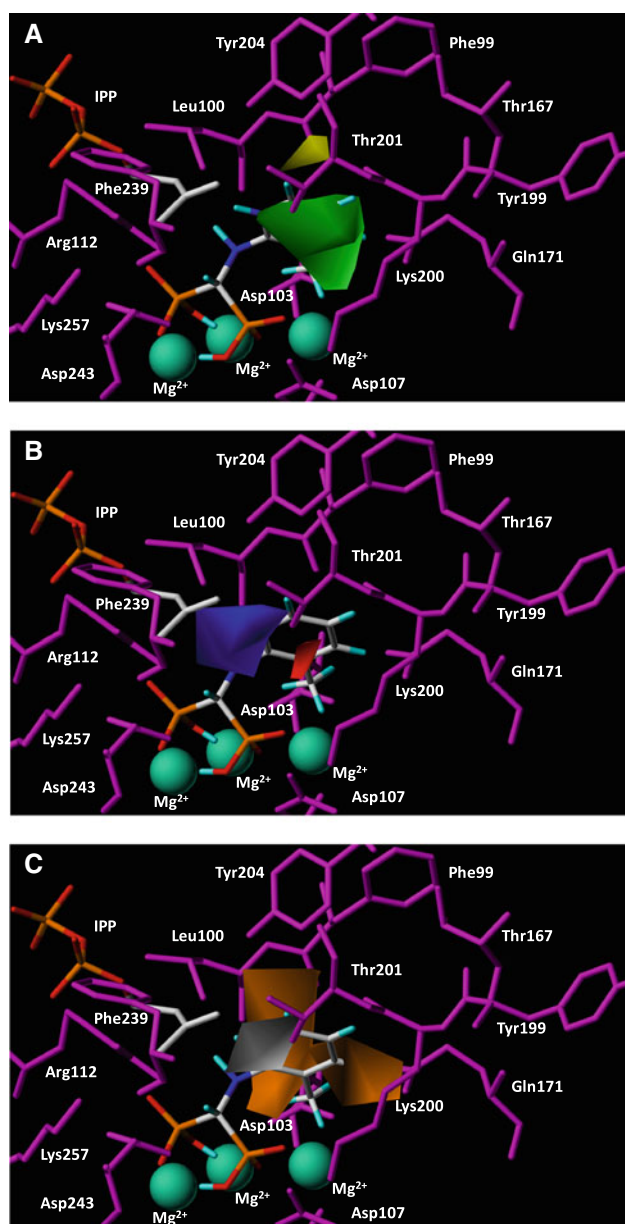
Fig. 8 Projection of molecule (19) and the contour maps of 3D-QSAR/CoMSIA model A4 obtained with final IC$_{50}$ values into the active site of human FPPS (PDB 2F8Z). **a** Steric contour map: *green regions* indicate where steric bulk is expected to enhance activity; *yellow regions* indicate where steric bulk is expected to reduce activity. **b** Electrostatic contour map: *red regions* indicate where positive charge in the molecule is expected to enhance activity; *blue region* indicate where negative charge in the molecule is expected to enhance activity. **c** Hydrophobic contour map: *orange regions* indicate where hydrophobic groups are expected to enhance activity; *grey region* indicates where hydrophobic groups are expected to reduce activity

charge (as can be the nitrogen protonation) has moved apart from Lys200 and Thr201, and this new localization could suggest the importance of delocalization of positive charge in the aromatic ring of the side chain to increase the biological activity of the NBPs. On the other hand, the
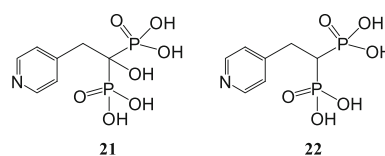
Scheme 3 Proposed molecules as potential inhibitor of human FPPS enzyme

electrostatic favourable region obtained for a negative charge or hydrogen bond acceptor (blue region) has been obtained over the aromatic nitrogen in pyridine in orto- and meta- positions. This region is close to the R$_1$ side chain, and indicates that the presence of a hydroxyl could increase the biological activity of the molecule.

The most important factor in CoMSIA model was the hydrophobic factor (49.0 %). Figure 8c shows favourable (orange) and unfavourable (grey) hydrophobic regions projected into the active site of the human FPPS enzyme. Hydrophobic contour maps show the favourable region oriented into the cavity of the enzyme, in agreement with the hydrophobicity nature of the cavity. This representation indicates that every hydrophobic side chain of NBPs oriented to the cavity will enhance the biological activity of the molecule.

The time-dependent inhibition is widely interpreted due to an isomerisation of the enzyme-inhibitor complex where the nitrogen moiety of NBPs plays an important role [11], and final IC$_{50}$ values of NBPs depend on the capacity of the molecule to hold the isomerisation state. Differences between initial and final 3D-QSAR models also suggest a rearrangement of the active site that involves changes of the molecular requirements to get a good inhibitor.

The analysis of the CoMSIA contour maps suggested that the possibility to form a hydrogen bond with Lys200 and Thr201 is not the only factor to explain the time-dependent inhibition of human FPPS. For example, the projection of molecule (19) into the active site of the FPPS did not show any hydrogen bond interaction of R$_2$ group with residues around it (Fig. 8). Nevertheless, molecule (19) presents the highest initial biological value (IC$_{50}$ = 75.2 nM) and also a high final biological activity (IC$_{50}$ = 6.7 nM).

Comparing pairs of molecules analogues with and without a hydroxyl group in R$_1$ side chain (7/9, 11/12 and 13/14) we observed that molecules with a hydroxyl group present lower final IC$_{50}$ values than their analogues with a hydrogen atom at R$_1$. In all cases, the presence of a hydroxyl group at R$_1$ causes a hydrogen bond interaction with carboxylate group of Asp243 and, as a consequence, it increases the stability of the enzyme-inhibitor complex.

Predictions

Nowadays, a high number of NBPs that have been used for the treatment of different diseases can also act as potential

inhibitors of the activity of the human enzyme FPPS. Such is the case of molecules (21) and (22) [59, 60] (scheme 3), that have been suggested for the treatment of Chagas' illness.

On order to test the robustness and utility of 3D-QSAR/CoMSIA model, it has been used to predict the unknown biological activity of these compounds. The final IC_{50} values obtained for molecules (21) and (22) are 10.2 nM ($pIC_{50} = 7.99$) and 22.6 nM ($pIC_{50} = 7.64$), respectively. Molecules (21) and (22) show some similar steric and electrostatic interactions to those shown in molecule (7) (final IC_{50} 5.7 nM). Molecule (21) has a hydroxyl group at R_1 and molecule (22) a hydrogen atom. As in all hydroxyl/hydrogen analogues pairs, the model predicts a better value of final IC_{50} value for the molecule with a hydroxyl group at R_1.

Predicted final IC_{50} values for (21) and (22) are similar or better than the well established NBPs used for the treatment of diseases associated with bone resorption (zoledronate, risedronate, pamidronate, etc.). Therefore, molecules with similar steric, electrostatic and hydrophobic parameters could be developed as potential inhibitors of human FPPS enzyme.

Conclusions

In this work, we constructed the first 3D-QSAR model for predicting the inhibitory ability of nitrogen BPs on human FPPS. The model assesses the relative significance of steric, electrostatic and hydrophobic factors towards predicting biological activity in this drug class.

The predictive ability of the 3D-QSAR model was found to rely on the choice of biologically active conformations and protonation states of the target molecules. Such conformations and specially protonation states provide an accurate predicted pIC_{50} values and a steric, electrostatic and hydrophobic contour map consistent with the interactions of the compounds into the active site of human FPPS.

The best 3D-QSAR model to predict initial biological activity values of NBPs was obtained with CoMFA analysis with model C4 ($q^2 = 0.725$ $r^2 = 0.957$, $N = 4$), although other models have similar statistical results. Model C4 revealed that the initial biological activity of the NBPs was more markedly dependent on steric interactions, which contributed 74.8 % to its predictive ability, than on electrostatic interactions, which contributed 25.2 % only. These results obtained with initial IC_{50} values suggested that the first step, the union of the inhibitor to the active site, is driven by the capacity of R_2 side chain to fit into the active site.

The union of NBPs to the active site yields an isomerisation of the structure of the active site enclosing the inhibitor. The rearrangement of the active site modifies the steric, electrostatic and hydrophobic requirement of the active site. The best 3D-QSAR model to predict final values of biological activity of NBPs, and to reproduce these requirements, was obtained with CoMSIA analysis for the model A4. This model revealed that final biological activity of NBPs was more dependent on hydrophobic interactions (49.0 %). However, steric (27.8 %) and electrostatic (23.2 %) factors also play an important role in the final biological activity. The presence of a hydroxyl group enhanced the biological activity of the NBPs. Projection of NBPs into the active site suggested a possible hydrogen bond interaction of the hydroxyl group with Asp243 that helps to hold the isomerized enzyme-inhibitor complex, increasing then the potency of the inhibitor with the time.

Finally, the electrostatic contribution to initial and final 3D-QSAR models is high enough to justify careful examination of the protonation status of the NBPs in the training set in order to assess its influence on the final result. Since atomic charges are not an experimental observable, different partitioning scheme have been considered to analyze how it affects to the QSAR model. In this system, mainly ruled by steric and hydrophobic factors, the protonation states improves the statistical results but the influence of the kind of atomic charges is rather small.

References

1. Fleisch H (1993) Editorial: prospective use of bisphosphonates in osteoporosis. J Clin Endocrinol Metab 76:1397–1398
2. Rodan GA (1998) Mechanisms of action of bisphosphonates. Annu Rev Pharmacol Toxicol 38:375–388
3. Martin MB, Arnold W, Heath HT III, Urbina JA, Oldfield E (1999) Nitrogen-containing bisphosphonates as carbocation transition state analogs for isoprenoid biosynthesis. Biochem Biophys Res Commun 263:754–758
4. Coleman RE (2005) Bisphosphonates in breast cancer. Ann Oncol 16:687–695
5. Sicard H, Al Saati T, Delsol G, Fournié JJ (2001) Synthetic phosphoantigens enhance human Vγ9 Vδ2T lymphocytes killing of non-Hodgkin's B lymphoma. Mol Med 7:711–722
6. Wilhelm M, Kunzmann V, Eckstein S, Reimer P, Weissinger F, Ruediger T, Tony HP (2003) γδT cells for immune therapy of patients with lymphoid malignancies. Blood 102:200–206
7. Stresing V, Daubiné F, Benzaid I, Mönkkönen H, Clézardin P (2007) Bisphosphonates in cancer therapy. Cancer Lett 257:16–35
8. Martin MB, Sanders JM, Kendrick H, Luca-Fradley K, Lewis JC, Grimley JS, Van Brussel EM, Olsen JR, Meints GA, Burzynska A, Kafarski P, Croft SL, Oldfield E (2002) Activity of bisphosphonates against trypanosoma brucei rhodesiense. J Med Chem 45:2904–2914
9. Dąbrowska E, Burzyńska A, Mucha A, Matczak-Jon E, Sawka-Dobrowolska W, Berlicki L, Kafarski P (2009) Insight into the mechanism of three component condensation leading to aminomethylenebisphosphonates. J Org Chem 694:3806–3813

10. Baojie Li B, Chau JFL, Wang X, Leong WF (2011) Bisphosphonates, specific inhibitors of osteoclast function and a class of drugs for osteoporosis therapy. J Cell Biochem 112:1229–1242

11. Dunford JE, Kwaasi AA, Rogers MJ, Barnett BL, Ebetino FH, Russell RGG, Oppermann U, Kavanagh KL (2008) Structure-activity relationships among the nitrogen containing bisphosphonates in clinical use and other analogues: time-dependent inhibition of human farnesyl pyrophosphate synthase. J Med Chem 51:2187–2195

12. Zhang FL, Casey PJ (1996) Protein prenylation: molecular mechanisms and functional consequences. Annu Rev Biochem 65:241–269

13. Sinensky M (2000) Recent advances in the study of prenylated proteins. Biochim Biophys Acta 1484:93–106

14. Shipman CM, Rogers MJ, Apperley JF, Russell RG, Croucher PI (1997) Bisphosphonates induce apoptosis in human myeloma cell lines; a novel anti-tumour activity. Br J Haematol 98:665–672

15. Russell RG, Xia Z, Dunford JE, Oppermann U, Kwaasi A, Hulley PA, Davanagh KL, Triffitt JT, Lundy MW, Phipps RJ, Barnett BL, Coxon FP, Rogers MJ, Watts NB, Ebetino FH (2007) Bisphosphonates: an update on mechanisms of action and how these relate to clinical efficacy. Ann N Y Acad Sci 1117:209–257

16. Zhang Y, Cao R, Yin F, Hudock MP, Guo R-T, Krysiak K, Mukherjee S, Gao Y-G, Robinson J, Song Y, No JH, Bergan K, Leon A, Cass L, Goddard A, Chang T-K, Lin F-Y, Van Beek E, Papapoulos S, Wang AH-J, Kubo T, Ochi M, Mukkamala D, Oldfield E (2009) Lipophilic bisphosphonates as dual farnesyl/geranylgeranyl diphosphate synthase inhibitors: an X-ray and NMR investigation. J Am Chem Soc 131:5153–5162

17. Frith JC, Mönkkönen J, Blackburn M, Russell RGG, Rogers MJ (1997) Clodronate and liposome-encapsulated clodronate are metabolized to a toxic ATP analog, adenosine 5'-(β, γ-dichloromethylene) triphosphate, by mammalian Cells in vitro. J Bone Miner Res 12:1358–1367

18. Tarshis LC, Yan M, Poulter CD, Sacchettini JC (1994) Crystal structure of recombinant farnesyl diphosphate synthase at 2.6-Å resolution. Biochemistry 33:10871–10877

19. Tarshis LC, Proteau P, Poulter CD, Sacchettini JC (1996) Regulation of product chain length by isoprenyl diphosphate synthases. Proc Natl Acad Sci 93:15018–15023

20. Gabelli SB, McLellan JS, Montalvetti A, Oldfield E, Docampo R, Amzel LM (2005) Structure and mechanism of the farnesyl diphosphate synthase from Trypanosoma cruzi: implications for drug design. Proteins 62:80–88

21. Kavanagh KL, Guo K, Dunford JE, Wu X, Knapp S, Ebetino FH, Rogers MJ, Russell RG, Oppermann U (2006) The molecular mechanism of nitrogen-containing bisphosphonates as antiosteoporosis drugs. Proc Natl Acad Sci 103:7829–7834

22. Rondeau JM, Bitsch F, Bourgier E, Geiser M, Hemming R, Kroemer M, Lehmann S, Ramage P, Rieffel S, Strauss A, Green JR, Jahnke W (2006) Structural basis for the exceptional in vivo efficacy of bisphosphonate drugs. ChemMedChem 1:267–273

23. Lin YS, Park J, De Schutter JW, Huang XF, Berghuis AM, Sebag M, Tsantrizos YS (2012) Design and synthesis of active site inhibitors of the human farnesyl pyrophosphate synthase: apoptosis and inhibition of ERK phosphorylation in multiple myeloma cells. J Med Chem 55:3201–3215

24. Szabo CM, Martin MB, Oldfield E (2002) An investigation of bone resorption and Dictyostelium discoideum growth inhibition by bisphosphonate drugs. J Med Chem 45:2894–2903

25. Sanders JM, Gómez AO, Mao J, Meints GA, Van Brussel EM, Burzynska A, Kafarski P, González-Pacanoska D, Oldfiel E (2003) 3D-QSAR investigation of the inhibition of leishmania major farnesyl pyrophosphate synthase by bisphosphonates. J Med Chem 46:5171–5183

26. Whitaker M, Guo J, Kehoe T, Benson G (2012) Perspective: bisphosphonates for osteoporosis - where do we go from here? N Engl J Med 366:2048–2051

27. Hess LM, Jeter JM, Benham-Hutchins M, Alberts DS (2008) Factors associated with osteonecrosis of the jaw among bisphophonates users. Am J Med 121:475–483

28. Bauss F, Pfister T, Papapoulos S (2008) Ibandronate uptake in the jaw is similar to long bones and vertebrae in the rat. J Bone Miner Metab 26:406–408

29. Ruggiero SL, Mehrotra B (2009) Bisphosphonate-related osteonecrosis of the jaw: diagnosis, prevention, and management. Annu Rev Med 60:85–96

30. Park-Wyllie LP, Mamdani MM, Juurlink DN, Hawker GA, Gunraj N, Austin PC, Whelan DB, Weiler JP, Laupacis A (2011) Bisphosphonate use and the risk of subtrochanteric or femoral shaft fractures in older women. JAMA 305:783–789

31. Cramer RD III, Patterson DE, Bunce JD (1988) Comparative molecular field analysis (CoMFA). 1. Effect of shape on binding of steroids to carrier proteins. J Am Chem Soc 110:5959–5967

32. Klebe G, Abraham U, Mietzner T (1994) Molecular similarity indices in a comparative analysis (CoMSIA) of drug molecules to correlate and predict their biological activity. J Med Chem 37:4130–4146

33. Kotsikorou E, Oldfield E (2003) A quantitative structure-activity relationship and pharmacophore modelling investigation of aryl-X and heterocyclic bisphosphonate as bone resorption agents. J Med Chem 46:2932–2944

34. Clark M, Cramer RD III, Van Opdenbosch N (1989) Validation of the general purpose Tripos 5.2 force field. J Comp Chem 10:982–1012

35. SYBYL 8.0 Tripos Inc., 1699 South Hanley Rd. St. Louis, Missouri, 63144-2917

36. NBO Version 3.1, Glendening ED, Reed AE, Carpenter JE, Weinhold F

37. Reed AE, Weinstock RB, Weinhold F (1985) Natural-population analysis. J Chem Phys 83:735–746

38. Reed AE, Curtiss LA, Weinhold F (1988) Intermolecular interactions from a natural bond orbital, donor-acceptor viewpoint. Chem Rev 88:899–926

39. Gaussian 09, Revision B.1, Frisch MJ, Trucks GW, Schlegel HB, Scuseria GE, Robb MA, Cheeseman JR, Scalmani G, Barone V, Mennucci B, Petersson GA, Nakatsuji H, Caricato M, Li X, Hratchian HP, Izmaylov AF, Bloino J, Zheng G, Sonnenberg JL, Hada M, Ehara M, Toyota K, Fukuda R, Hasegawa J, Ishida M, Nakajima T, Honda Y, Kitao O, Nakai H, Vreven T, Montgomery Jr. JA, Peralta JE, Ogliaro F, Bearpark M, Heyd JJ, Brothers E, Kudin KN, Staroverov VN, Kobayashi R, Normand J, Raghavachari K, Rendell A, Burant J. C, Iyengar SS, Tomasi J, Cossi M, Rega N, Millam JM, Klene M, Knox JE, Cross JB, Bakken V, Adamo C, Jaramillo J, Gomperts R, Stratmann RE, Yazyev O, Austin AJ, Cammi R, Pomelli C, Ochterski JW, Martin RL, Morokuma K, Zakrzewski VG, Voth GA, Salvador P, Dannenberg JJ, Dapprich S, Daniels AD, Farkas Ö, Foresman JB, Ortiz JV, Cioslowski J, Fox DJ. Gaussian, Inc., Wallingford CT, 2009

40. Weinhold FA (1997) Nature of H-bonding in clusters, liquids, and enzymes: an ab initio, natural bond orbital perspective. J Mol Struct (Theochem) 398:181–197

41. Kubinyi H (1998) Comparative molecular field analysis (CoMFA). In: Schleyer PvR, Allinger NL, Clark T, Gasteiger J, Kollman PA, Schaefer III HF, Schreiner PR (eds) The encyclopedia of computational chemistry, vol 1. Wiley, Chichester, p 448–460

42. Viswanadhan VN, Ghose AK, Revankar GR, Robins RK (1989) Atomic physicochemical parameters for three dimensional structure directed quantitative structure-activity relationships. 4. Additional parameters for hydrophobic and dispersive interactions and their

application for an automated superposition of certain naturally occurring nucleoside antibiotics. J Chem Inf Comput Sci 29: 163–172

43. Geladi P, Kowalski B (1986) Partial least-squares regression: a tutorial. Anal Chim Acta 185:1–17

44. Hasegawa K, Funatsu K (2000) Partial least squares modelling and genetic algorithm optimization in quantitative structure-activity relationships. SAR QSAR Environ Res 11:189–209

45. Wold S (1978) Cross-validatory estimation of the number of components in factor and principal components models. Technometrics 20:397–406

46. MarvinSketch 5.7, Calculator Plugin and Chemical Terms Demo Copyright © 1999–2012 ChemAxon Ltd

47. SPARC Performs Automated Reasoning in Chemistry. Sparc v4.6

48. Haynes WM (2012) CRC Handbook of Chemistry and Physics 93th edn. Taylor & Francis Group

49. Walba H, Isensee RW (1961) Acidity constants of some arylimidazoles and their cations. J Org Chem 26:289–2791

50. Golbraikh A, Tropsha A (2002) Beware of q2! J Mol Graph Model 20:267–276

51. Gasteiger J, Marsili M (1980) Iterative partial equalization of orbital electronegativity: a rapid access to atomic charges. Tetrahedron 36:3219–3228

52. Marsili M, Gasteiger J (1980) π Charge distribution from molecular topology and π orbital electronegativity. Croat Chem Acta 53:601–614

53. Montgomery JA Jr, Frisch MJ, Ochterski JW, Petersson GA (1999) A complete basis set model chemistry. VI. Use of density functional geometries and frequencies. J Chem Phys 110: 2822–2827

54. Montgomery JA Jr, Frisch MJ, Ochterski JW, Petersson GA (2000) A complete basis set model chemistry. VII. Use of the minimum population localization method. J Chem Phys 112: 6532–6542

55. Singh UC, Kollman PA (1984) An approach to computing electrostatic charges for molecules. J Comp Chem 5:129–145

56. Besler BH, Merz KM Jr, Kollman PA (1990) Atomic charges derived from semiempirical methods. J Comp Chem 11:431–439

57. Breneman CM, Wiberg KB (1990) Determining atom-centered monopoles from molecular electrostatic potentials. The need for high sampling density in formamide conformational analysis. J Comp Chem 11:361–373

58. Ohno K, Mori K, Orita M, Takeuchi M (2011) Computational insights into binding of bisphosphates to farnesyl pyrophosphate synthase. Curr Med Chem 18:220–233

59. Sanz-Rodríguez CE, Concepción JL, Pekerar S, Oldfield E, Urbina JA (2007) Bisphosphonates as inhibitors of trypanosoma cruzi hexokinase: kinetic and metabolic studies. J Biol Chem 282:12377–12387

60. Feng-Lei W, Rong-Xin Y, Ji-Min X (2011) 4-[2-(Hydrogen phosphonate)-2-hydroxy-2-phosphonoethyl]pyridinium. Acta Cryst. E 67:o1025